Hepatobiliary & Pancreatic Diseases International 18 (2019) 164–172

Contents lists available at ScienceDirect

Hepatobiliary & Pancreatic Diseases International

journal homepage: www.elsevier.com/locate/hbpd

Original Article/Liver

^{18}F-fluoromisonidazole positron emission tomography may be applicable in the evaluation of colorectal cancer liver metastasis

Ming-Yu Zhang[a], Rong-Jun Zhang[b], Hui-Jie Jiang[a,*], Hao Jiang[a], Hai-Long Xu[a], Wen-Bin Pan[a], Yi-Qiao Wang[a], Xin Li[a]

[a] *Department of Radiology, the Second Affiliated Hospital of Harbin Medical University, Harbin 150086, China*
[b] *Key Laboratory of Nuclear Medicine of the Ministry of Health, Jiangsu Key Laboratory of Molecular Nuclear Medicine, Jiangsu Institute of Nuclear Medicine, Wuxi 214063, China*

ARTICLE INFO

Article history:
Received 27 September 2018
Accepted 12 February 2019
Available online 26 February 2019

Keywords:
^{18}F-FMISO
Positron emission tomography
Colorectal liver metastases
Heterogeneity

ABSTRACT

Background: Positron emission tomography (PET) imaging is a non-invasive functional imaging method used to reflect tumor spatial information, and to provide biological characteristics of tumor progression. The aim of this study was to focus on the application of ^{18}F-fluoromisonidazole (FMISO) PET quantitative parameter of maximum standardized uptake value (SUVmax) ratio to detect the liver metastatic potential of human colorectal cancer (CRC) in mice.

Methods: Colorectal liver metastases (CRLM) xenograft models were established by injecting tumor cells (LoVo, HT29 and HCT116) into spleen of mice, tumor-bearing xenograft models were established by subcutaneously injecting tumor cells in the right left flank of mice. Wound healing assays were performed to examine the ability of cell migration *in vitro*. ^{18}F-FMISO uptake in CRC cell lines was measured by cellular uptake assay. ^{18}F-FMISO-based micro-PET imaging of CRLM and tumor-bearing mice was performed and quantified by tumor-to-liver SUVmax ratio. The correlation between the ^{18}F-FMISO SUVmax ratio, liver metastases number, hypoxia-induced factor 1α (HIF-1α) and serum starvation-induced glucose transporter 1 (GLUT-1) was evaluated using Pearson correlation analysis.

Results: Compared with HT29 and HCT116, LoVo-CRLM mice had significantly higher liver metastases ratio and shorter median survival time. LoVo cells exhibited stronger migration capacity and higher radiotracer uptake compared with HT29 and HCT116 in *in vitro*. Moreover, ^{18}F-FMISO SUVmax ratio was significantly higher in both LoVo-CRLM model and LoVo-bearing tumor model compared to models established using HT29 and HCT116. In addition, Pearson correlation analysis revealed a significant correlation between ^{18}F-FMISO SUVmax ratio of CRLM mice and number of liver metastases larger than 0.5 cm, as well as between ^{18}F-FMISO SUVmax ratio and HIF-1α or GLUT-1 expression in tumor-bearing tissues.

Conclusions: ^{18}F-FMISO parameter of SUVmax ratio may provide useful tumor biological information in mice with CRLM, thus allowing for better prediction of CRLM and yielding useful radioactive markers for predicting liver metastasis potential in CRC.

Introduction

Colorectal cancer (CRC) is the third most commonly diagnosed malignancy worldwide [1]. The liver is the most common site of CRC metastasis that has a decisive role in patient's survival [2]. Tumor metastasis depends on tumor genetic and microenvironmental heterogeneity; tumor heterogeneity is associated with different biological behavior, clinical presentation, prognosis and individual therapy responses [3,4]. Currently, more and more individualized treatment of patients with CRC has highlighted the need for functional imaging methods to further explore the CRC biological behavior in real-time.

The characteristic biological behavior of radiotracer uptake depicts the process by which the tracer is transported into the tissue, thereby reflecting tumor-related biological specifics in the living state. Hypoxic regions are present in majority of malignant solid tumors because tumor cells have a tendency to grow very rapidly leading to insufficient oxygen supply [5]. Nevertheless, hypoxic tumors have shown to be associated with poor prognosis, aggressive phenotype, angiogenesis, tumor invasion and metastasis, and resistance to chemotherapy and radiotherapy [6,7]. The

* Corresponding author.
E-mail address: jhjemail@163.com (H.-J. Jiang).

https://doi.org/10.1016/j.hbpd.2019.02.008

different levels of hypoxia and the distribution of hypoxic regions in tumors lead to different metastatic potential in different CRC patients [8]. Non-invasive and dynamic assessments of tumor hypoxia variability promote comprehension of tumor biological behavior at the molecular level. Positron emission tomography (PET) imaging is a non-invasive functional imaging method used to reflect the tumor structure and dynamic function, while the parameters of PET can provide information related to tumor spatial heterogeneity which are very useful for selecting the appropriate therapy early in the personalized approach process [9,10]. The application of ^{18}F-fluoromisonidazole (^{18}F-FMISO) PET imaging for detection of tumor hypoxia continues to be the leading radiopharmaceutical for the evaluation, prognostication and quantification of hypoxia [11,12]. FMISO is less confounded by blood flow and its uptake after 2 h is an accurate reflection of inadequate regional PO_2 at the time of radiopharmaceutical administration. ^{18}F-FMISO PET imaging is considered the most promising method for hypoxia quantification since the tracer binds in hypoxic cells selectively [11,13]. The lipophilic nature of ^{18}F-FMISO ensures facile cell-membrane penetration and diffusion into tissue. In addition, a previous study [14] has shown that ^{18}F-FMISO can accumulate in a solid tumor with oxygen level of $\leq$ 10 mmHg. The ^{18}F-FMISO radioactive parameter of standard uptake value (SUV) can be used for quantification of the intratumoral hypoxia levels while ^{18}F-FMISO PET images can reflect the distribution of tumor hypoxia region. The clinical application of ^{18}F-FMISO radiotracer has been done on glioblastoma multiforme including differential diagnosis, assessing the biological aggressiveness region and prognostic prediction of breast cancer, lung cancer, and head and neck cancer [15–19]. Currently, there are only few studies on the application of ^{18}F-FMISO PET tracers for quantification of heterogeneity in mice with human CRC xenograft.

The aim of this study was to investigate biological behavior (primarily, its metastasis to the liver) of different CRC cell lines LoVo (derived from metastatic site), HT29 and HCT116 (both cells derived from primary tumor site), as well as to explore the diversity of ^{18}F-FMISO uptake and tumor-related biomarker *in vitro* and *in vivo,* using a mice model. These findings may contribute to the better understanding of biological behavior of CRC and to yielding useful radioactive markers necessary to guide personalized therapeutic regimen.

Methods

Cell cultures

The human CRC cell lines LoVo, HT29 and HCT116 were purchased from the Type Culture Collection of the Chinese Academy of Sciences (Shanghai, China). The LoVo cell line was maintained in Dulbecco's Modified Eagle Medium (DMEM, Gibco Corporation, Waltham, USA), while HT29 and HCT116 were cultured in McCoy's 5A medium (Gibco Corporation); all media were supplemented with 10% fetal bovine serum (Hyclone, Logan, USA) and 1% penicillin-streptomycin (Beyotime Biotechnology, Shanghai, China). All cells were cultured in a humidified atmosphere containing 5% CO_2 / 95% air at 37 °C.

For hypoxia experiment, three types of cells were cultured in a modulator incubator chamber at 37 °C with 1% O_2, 5% CO_2 and 94% N_2 at 37 °C atmosphere for 24 h.

CRLM and xenograft mice models

Five-week-old female BALA/C nude mice (weighing 16–18 g) were purchased from Animal Laboratory of Cavens Corporate of Changzhou (Changzhou, China). All animals were housed in an environment with temperature of 22 ± 1 °C, relative humidity of 50% ± 1% and a light/dark cycle of 12 h/12 h. All animal studies (including the mice euthanasia procedure) were done in compliance with the regulations and guidelines of Jiangsu Institute of Nuclear Medicine institutional animal care and were conducted according to the Association for Assessment and Accreditation of Laboratory Animal Care and the Institutional Animal Care and Use Committee guidelines.

Sixty colorectal liver metastases (CRLM) xenograft models were established by injecting LoVo, HT29 or HCT116 cells (5.0×10^6 cells in 0.15 mL of phosphate-buffered saline) into spleen of anesthetized (2% isoflurane in pure oxygen) mice, respectively ($n = 20$). Additional eighteen tumor-bearing xenograft models were established by subcutaneously injecting LoVo cells, HT29 cells or HCT116 cells (5.0×10^6 cells in 0.15 mL of phosphate-buffered saline) in the right left flank, respectively ($n = 6$). After injection, the body weight and tumor volume of nude mice was recorded every three days. The mice were sacrificed after the micro-PET imaging was performed.

Cellular uptake in vitro

LoVo, HT29 and HCT116 cells were maintained in corresponding medium at 37 °C in a 1% O_2 hypoxia atmosphere for 24 h before ^{18}F-FMISO cellular uptake. The cells, ^{18}F-FMISO and buffer (DMEM containing 0.2% bovine serum albumin) were mixed into a glass test tube (2 mL) and incubated at 37 °C for 30, 60, 120 and 240 min, respectively. The tubes were divided in three groups: Group O, was composed of 100 μL radionuclides and 200 μL buffer (DMEM buffer with 0.2% bovine serum albumin) and was used as a control tube; Group T, contained 100 μL radionuclides which were used to measure the radionuclide dose; Group X, was composed of 100 μL radionuclides, 100 μL cell suspension and 100 μL DMEM buffer. The cellular uptake was normalized to 5×10^5 cells/tube; each cell line was tested three times at each time point. After incubation, O and X groups were centrifuged at 1000 rpm for 5 min and the supernatants were removed. The radioactivity of each cell line at different time point was accurately measured using Automatic Gamma Counter (PerkinElmer 2480, Waltham, MA, USA). The cellular uptake ratio was calculated using the following formula: X(cpm)-O(cpm)/T(cpm)%. cpm: counts per minute. The experiments were independently repeated three times.

Synthesis of ^{18}F-FMISO

^{18}F-FMISO were automatically synthesized with a multifunctional module (Wuxi Jiangyuan Industrial Technology and Trade Corporation, Wuxi, China) according to the previous report [20]. The final radiochemical purity of ^{18}F-FMISO was greater than 95%, while the specific activity was > 0.5 TBq/mmol. The ^{18}F-labeled tracers were formulated in normal saline and passed through a 0.22 μm Millipore filter for animal use.

Micro-PET imaging

^{18}F-FMISO PET imaging of LoVo, HT29 and HCT116 CRLM mice models ($n = 20$) were performed seven weeks after implantation. ^{18}F-FMISO PET imaging of LoVo, HT29 and HCT116 tumor-bearing models ($n = 6$) were performed when the tumor reached a volume of 1 cm^3. Prior to imaging, all the mice were anesthetized with 2% isoflurane in 100% oxygen with a flow rate of 1 L/min prior and images were acquired 4 h (radiopharmaceutical administration time in mice) after injection of ^{18}F-FMISO (about 14.8 MBq, 400 μCi) via tail vein. Micro-PET scans were acquired in 3-dimensional mode using an Inveon micro-PET scanner (Siemens Medical Solutions, Erlangen, Germany) with an ordered-subset expectation maximization/maximum: matrix, 128 × 128 × 159;

pixel size, 0.86 × 0.86 × 0.8 mm; β-value, 1.5, with uniform resolution. PET images were reconstructed and postprocessed using Inveon Acquisition Workplace software (version 2.0, Siemens Preclinical Solutions). During the whole process, mice body temperature was maintained using a heat lamp.

All micro-PET imaging procedures were conducted according to protocol approved by the Jiangsu Institute of Nuclear Medicine Animal Care and Use Committee.

Image analysis

Regions of interests (ROIs) were drawn on images around the entire liver metastasis or tumor-bearing lesions volume and background (normal liver tissue) using ASI Pro VM 6.8.6.9 software (Concorde Microsystems, Knoxville, TN, USA). ^{18}F-FMISO PET quantitative parameter of the maximum SUV (SUVmax) ratio was calculated as the tumor to liver SUVmax (T/L ratio). The calculation formulas for SUVmax were performed as: SUVmax = [Max × 8000 μCi/mL × weight (g)]/Injected dose μCi.

Wound healing assay

LoVo, HT29 and HCT116 cells were seeded in 6-well plates at a density of 5×10^5 cells/mL and were cultured until reaching monolayer confluency. The monolayer of cells was scratched with a 10 μL pipette tip to create a wound gap, followed by taking the first (0 h) picture with an Olympus IX71 microscope (Olympus, Tokyo, Japan). After first imaging cells were treated with 2% fetal bovine serum-containing medium and imaged 24 and 48 h after scratching, the wounded area was measured using Image-J software (NIH, Bethesda, MD, USA). Wound healing percentage was calculated with the following formula: wound healing percentage = (wounded area at 0 h − wounded area at indicated time)/wounded area at 0 h × 100%. This experiment was run in triplicate.

Immunofluorescence assay

LoVo, HT29 and HCT116 cells were seeded in 6-well plates until reaching appropriate densities. Cells were cultured in a modular incubator chamber at 37 °C in a hypoxic atmosphere of 1% O_2 for 24 h prior hypoxia-induced factor 1α (HIF-1α) staining and were serum-starved for 24 h prior to glucose transporter 1 (GLUT-1) staining. Cells were then washed with phosphate buffer saline three times and fixed with 4% paraformaldehyde for 30 min at room temperature, followed by incubation with 1% Triton X-100 for 15 min at room temperature. Subsequently, non-specific antibody binging sites were blocked with 10% normal goat serum for 30 min, and cells were incubated with anti-HIF-1α (1:100; H1alpha67; Abcam, Cambridge, UK) or anti-GLUT-1 (1:100; ab40084; Abcam) [21]. Images were taken with a confocal microscope (C2si; Nikon, Tokyo, Japan). The protein expression was quantified using Live Cell Imaging System (NIS-Elements, Tokyo, Japan).

Immunohistochemical staining

The tumor-bearing specimens were fixed in 10% formalin for 48 h, paraffin-embedded, and cut into 3 μm-thick sections. Immunohistochemical staining was performed as previously described [22]. Briefly, the slides were incubated with anti-HIF-1α (1:100; Abcam) or anti-GLUT-1 (1:100; Abcam) at 4 °C overnight. Next, the slides were incubated with HRP-labeled goat anti-mouse secondary antibody (Boster, Wuhan, China) at room temperature for 1 h followed by counterstaining with hematoxylin. The staining was observed under a BX53 Olympus microscope (Olympus) at magnification × 200. The brown-yellow staining levels of HIF-1α or GLUT-1 proteins were evaluated by Image-J software (NIH).

Statistical analysis

All data were expressed as mean ± standard deviation or frequency. Statistical analysis was performed using SPSS software (version 19.0, IBM, Armonk, NY, USA). The difference between three groups was assessed using one-way ANOVA with least-significant difference (LSD) test. The Fisher's exact test was used for comparing differences in liver metastatic potential. The correlation between the ^{18}F-FMISO parameters of SUVmax ratio and number of liver metastases, as well as tumor marker was analyzed using Pearson correlation analysis. A P value < 0.05 was considered statistically significant.

Results

LoVo cells are more prone to migration in vitro compared to HT29 and HCT116 cells

As shown in Fig. 1, the percentages of wound closure in LoVo cells (25.27% ± 0.6% at 24 h and 67.3% ± 0.51% at 48 h) at

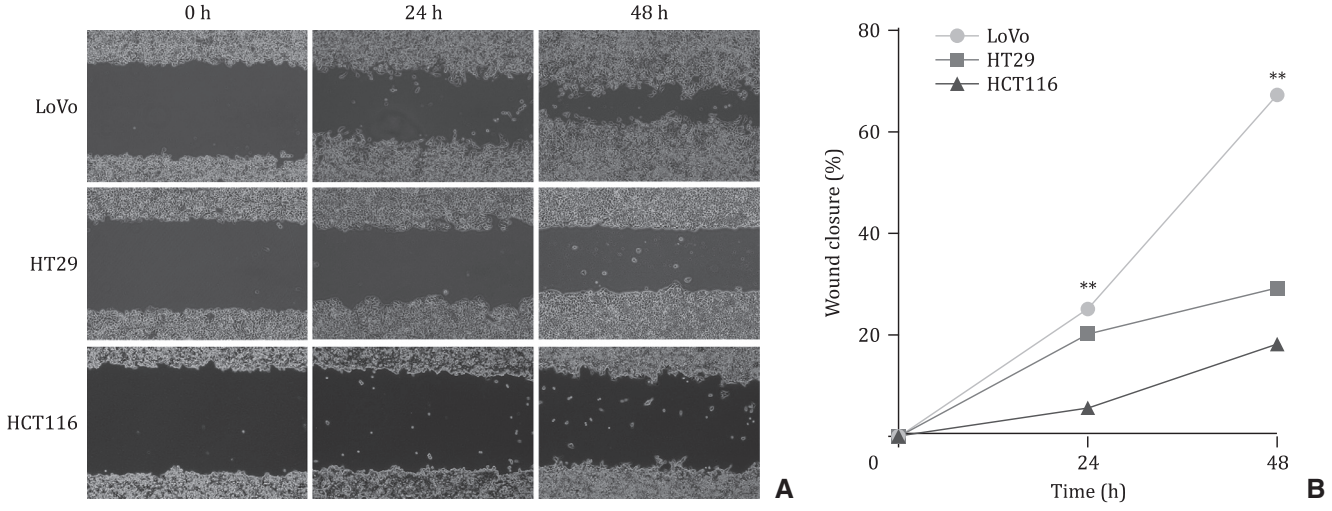

Fig. 1. Migratory capability of LoVo, HT29 and HCT116 cells *in vitro*. **A:** LoVo, HT29 and HCT116 cell monolayers were scratched using 10 μL pipette tips. The images were acquired at 0, 24 and 48 h after wound formation (original magnification × 100); **B:** Quantification of cell wound closure (%) of LoVo, HT29 and HCT116 cells. ** $P < 0.001$.

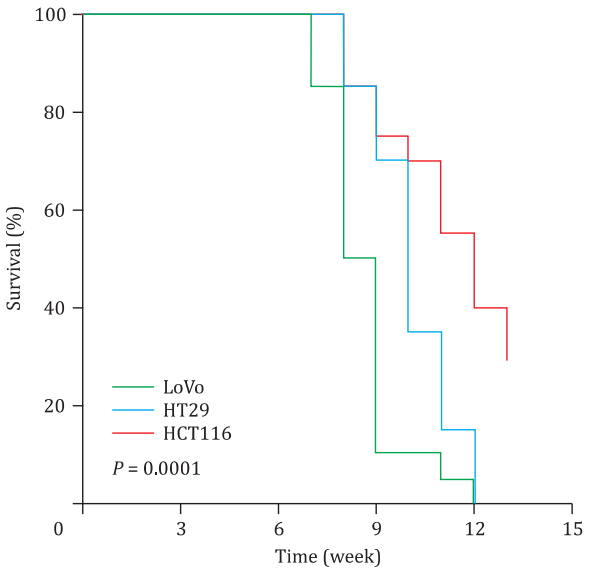

Fig. 2. Survival curves of LoVo, HT29 and HCT116-xenograft models ($n = 20$ per group).

different time points were higher compared to those in HT29 cells (20.46% ± 0.57% at 24 h and 29.32% ± 0.43% at 48 h, respectively; $P < 0.001$) and HCT116 cells (5.88% ± 0.83% at 24 h and 18.42% ± 0.73% at 48 h, respectively; $P < 0.001$).

LoVo cells have higher liver metastatic potential compared to HT29 and HCT116 cells

Twelve out of 20 LoVo-CRLM mice (60%), seven out of 20 HT29-CRLM mice (35%) and three out of 20 HCT116-CRLM mice (15%) had liver metastases ($\chi^2 = 8.756$, $P = 0.13$). In total, there were 22 mice with liver metastases of which 16 mice had liver metastasis lesions larger than 0.5 cm and a total of 35 liver metastasis nodules larger than 0.5 cm confirmed by anatomical measurement. In addition, the median survival time of LoVo, HT29 and HCT116-xenografted mice were 8.5, 10 and 12 weeks, respectively ($P = 0.0001$; Fig. 2). Moreover, HCT116-CRLM mice have significantly longer survival time compared to those of LoVo and HT29-xenografted mice.

In vitro cellular ^{18}F-FMISO uptake analysis of different CRC cell line

^{18}F-FMISO was taken up into LoVo, HT29 and HCT116 cells in a time-dependent manner. There was no statistical difference in ^{18}F-FMISO cellular uptake among LoVo, HT29 and HCT116 cells at 30 min ($P > 0.05$), while at 60 and 120 min, LoVo cells exhibited a significantly higher uptake compared to HT29 and HCT116 cells (all $P < 0.01$, Fig. 3). HT29 cells had a higher uptake of ^{18}F-FMISO than HCT116 at 60 and 120 min, however, these results were not statistically different ($P = 0.265$ and 0.462, respectively). It is noteworthy that there was a significant difference between each of LoVo, HT29 and HCT116 cells at 240 min (4.23 ± 0.13, 3.34 ± 0.18 and 2.22 ± 0.23, respectively, $P < 0.01$).

Expression of hypoxia-induced HIF-1α and serum starvation-induced GLUT-1 in LoVo, HT29 and HCT116 cells

HIF-1α and GLUT-1, tumor markers, had stronger fluorescent staining in hypoxia environment cultured LoVo cells than in HT29 and HCT116 cells ($P < 0.001$, Fig. 4). HT29 cells have a slightly higher fluorescent staining of HIF-1α and GLUT-1 than HCT116 cells; however, there was no statistical difference ($P > 0.05$). In addition, GLUT-1 and HIF-1α protein was strongly stained in LoVo tumor-bearing tissues compared with HT29 and HCT116 tumor tissues. GLUT-1, but not HIF-1α protein, was stronger in HT29 cells compared to HCT116 cells ($P < 0.01$).

^{18}F-FMISO quantitative parameter of SUVmax ratio can be used to distinguish the metastatic ability of different CRC cells in vivo

Our results show that liver metastases lesions larger than 0.5 cm could be detected by ^{18}F-FMISO-based micro-PET (Fig. 5) since the lesions contours were significantly clearer compared to lesions with contours less than 0.5 cm. SUVmax ratio of tumor-bearing tissues was higher than that of liver metastases tissues (LoVo: 1.97 ± 0.15 vs. 1.74 ± 0.15, $P < 0.05$; HT29: 1.72 ± 0.12 vs. 1.61 ± 0.18, $P < 0.05$; HCT116: 1.55 ± 0.09 vs. 1.38 ± 0.07, $P < 0.05$). On the other hand, SUVmax ratio of ^{18}F-FMISO both in LoVo-CRLM tumors and LoVo-tumor-bearing were significantly higher compared to HT29 and HCT116 ($P < 0.001$, Table 1). These results suggested that ^{18}F-FMISO quantitative parameter of SUVmax ratio could be used to distinguish the liver metastatic biological behavior of CRC in mice.

Correlation analysis

^{18}F-FMISO SUVmax ratio is significantly correlated with the protein expressions tumor biomarkers *in vivo* (HIF-1α, $r = 0.8145$, $P = 0.0075$; GLUT-1, $r = 0.8252$, $P = 0.0062$) and number of liver metastases larger than 0.5 cm ($r = 0.6408$, $P = 0.0013$, Fig. 6).

Discussion

CRC is the third most common cancer diagnosed in both men and women. Approximately, 25% patients have synchronous colorectal liver metastases at the time of initial presentation and 50% patients develop metachronous liver metastases within 3 years after the primary lesion resection [23,24]. Liver metastasis remains a leading cause of CRC-related mortality. Kim and colleagues have shown that the genetic intra-tumor heterogeneity is prevalent in CRC serving as a potential driving force to generate metastasis-initiating clones [25]. In addition, inter-tumor heterogeneity may be relevant for tumor progression, metastasis, prognosis and treatment selection [26,27]. Therefore, a better comprehension of the CRC metastasis-associated biological behavior using an imaging

Table 1
Comparison of ^{18}F-FMISO SUVmax ratio between LoVo, HT29 and HCT116 mice models.

Variables	Cell lines			*P* value
	LoVo	HT29	HCT116	
No. (CRLM tumor size > 0.5 cm)	19	12	4	
CRLM models SUVmax ratio	1.74 ± 0.15	1.61 ± 0.18	1.38 ± 0.07	**< 0.001**
No. (tumor-bearing)	6	6	6	
Bearing-tumor models SUVmax ratio	1.97 ± 0.15	1.72 ± 0.12	1.55 ± 0.09	**< 0.001**

^{18}F-FMISO: ^{18}F-fluoromisonidazole; SUVmax: maximum standardized uptake value; CRLM: colorectal liver metastasis.

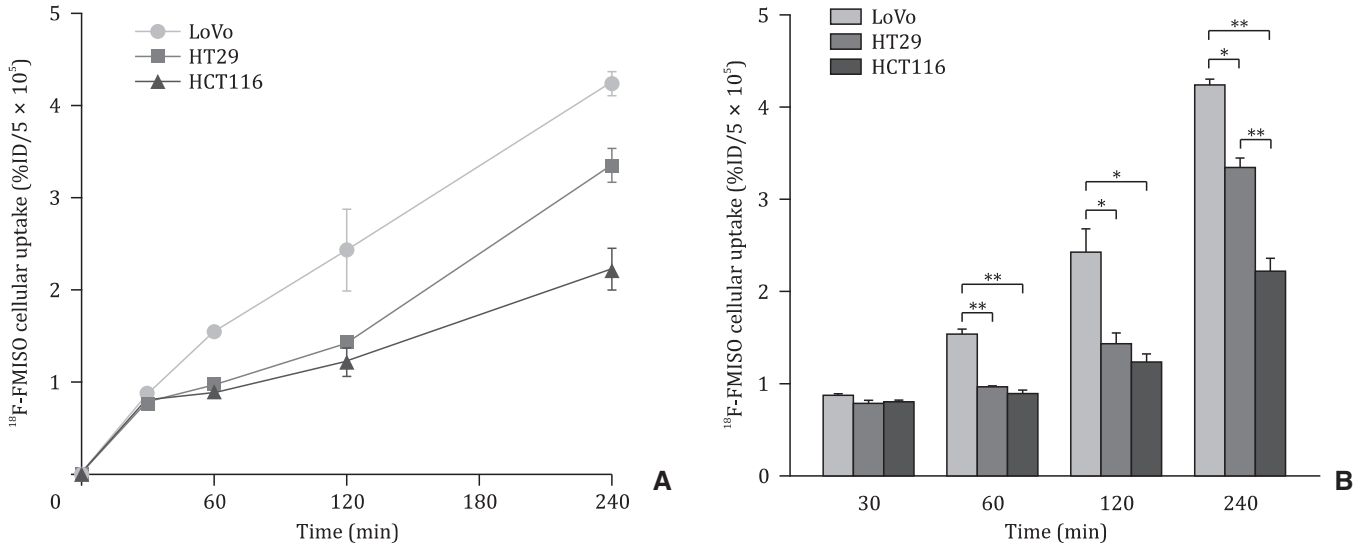

Fig. 3. *In vitro* cellular ^{18}F-FMISO uptake analysis of CRC cell lines. **A:** Time courses of *in vitro* cellular uptake of ^{18}F-FMISO in LoVo, HT29 and HCT116 cells. **B:** The quantitative histogram of ^{18}F-FMISO cellular uptake. Cells were incubated with ^{18}F-FMISO for 30, 60, 120, and 240 min, respectively. The percentage of the injected dose (%ID) of ^{18}F-FMISO per 5×10^5 cells. Data are expressed as the mean ± standard deviation, * $P < 0.01$; ** $P < 0.001$.

biomarker is crucial for early detection of liver metastases and for selection of individualized treatment in CRC patients.

Biological behavioral differences in CRC tumor cells lead to altered microenvironments. Hypoxia micro-environmental factor is a dynamic process across the progression of the tumor associated with angiogenesis, tumor vascularization, invasion, metastasis and drug resistance in CRC [8,28]. Nuclear imaging techniques of PET could quantify tissue uptake of tracer such as ^{18}F-FMISO and non-invasively reveal the hypoxic region location of the tumor. Two hours after radiotracer injection, ^{18}F-FMISO uptake in a solid tumor reflects the degree of hypoxia and hence the changes affecting the malignant biological behavior [11,29]. In this study, we firstly compared the migratory capability between three lines of CRC cells (LoVo, HT29 and HCT116) using wound healing assay. The obtained results confirmed that LoVo cells exhibited a stronger migratory capability followed by HT29 and HCT116. The incidence of liver metastasis in LoVo-CRLM mice was higher compared to those of HT29 and HCT116 CRLM mice. In addition, the median survival time in LoVo CRLM mice was 1.5 weeks shorter than HT29 CRLM mice and 3.5 weeks shorter than HCT116 CRLM mice. The difference in cell migration, tumor metastasis, and survival time in CRLM mice demonstrated the diversity of biological behavior among CRC cell lines or tumors.

We selected ^{18}F-FMISO tracer as the PET marker for hypoxia detection and used its image data to quantify the tumor biological difference in CRLM and CRC tumor-bearing mice. For ^{18}F-FMISO *in vitro* cellular uptake, LoVo, HT29 and HCT116 cells appeared to be time-dependent in a hypoxia-induced environment that allowed us to further establish a basis for detection of diversity in biological behaviors by PET *in vivo*. In order to better reflect the tumor spatial information related to CRC mice, we decided to conduct PET imaging 4 h after ^{18}F-FMISO injection, which was the time of highest uptake value *in vitro*. For CRLM mice images, the location information of liver metastases corresponded with anatomical position; however it was not possible to evaluate the hypoxia level in different CRLM mice subjectively and hence it was necessary to measure the SUVmax value of ROI for quantification of tumor biological behavior. The obtained results showed that ^{18}F-FMISO SUVmax ratio can be used to distinguish the differences in biological behavior between LoVo, HT29 and HCT116 CRLM mice. In order to avoid the detection limitation caused by small tumor volume, we established tumor-bearing mice for accurate quantification of image data. Our results showed that tumor-bearing PET images were more precise in displaying the distribution of hypoxic regions in tumor tissues, which allowed for subjective preliminary analysis of the activity levels of tumor tissues. The overall SUVmax ratio of ^{18}F-FMISO in tumor-bearing tissues were higher than CRLM ones; in addition, LoVo-tumor-bearing tissue had the highest SUVmax ratio, followed by HT29 and HCT116. The results of this experiment confirmed that ^{18}F-FMISO could be used to discriminate LoVo, HT29 and HCT116 cells and corresponding mice models. The high uptake in LoVo cells and tissues can be interpreted as the uptake of ^{18}F-FMISO in tumor cells representing tumor hypoxia levels, which in turn are related to the malignant biological behavior [14,30].

HIF-1α, a hypoxia-related protein, and GLUT-1, a HIF-1α-inducible protein in malignant tumor, are both associated with tumor progression and metastasis [31,32]. Estrella et al. [33] have shown that tumor cells with high glucose metabolism rates promote local invasive growth and metastasis due to the acidic pH environment. In addition, the immunohistochemical results have shown that high expression of GLUT-1 is localized to tumor cells in invasive regions. In our experiment, a stronger staining of HIF-1α and GLUT-1 were observed in LoVo cells and tissues compared to HT29 and HCT116 ones. This could be because the tumor is composed of heterogeneous components and the biology markers are heterogeneously expressed [31]. LoVo cells, which are derived from colorectal adenocarcinoma metastasis lesion have malignant biological character, and according to our correlation analysis, ^{18}F-FMISO SUVmax ratio in CRLM mice was significantly correlated with the liver metastases larger than 0.5 cm ($r = 0.6408$, $P = 0.0013$). As previously stated, hypoxia creates a nurturing environment for tumor progression and the evolution of metastatic, and malignant tumor with high metastases potential would promoted ^{18}F-FMISO uptake [14,32]. Similar results were reported by a meta-analysis of PET studies which has demonstrated a common tendency towards poorer outcome in tumors showing higher hypoxia tracer accumulation [34]. The present study also reported a correlation between ^{18}F-FMISO SUVmax ratio and HIF-1α or GLUT-1 expression in tumor-bearing tissues. This finding suggested that ^{18}F-FMISO SUVmax ratio might be used to

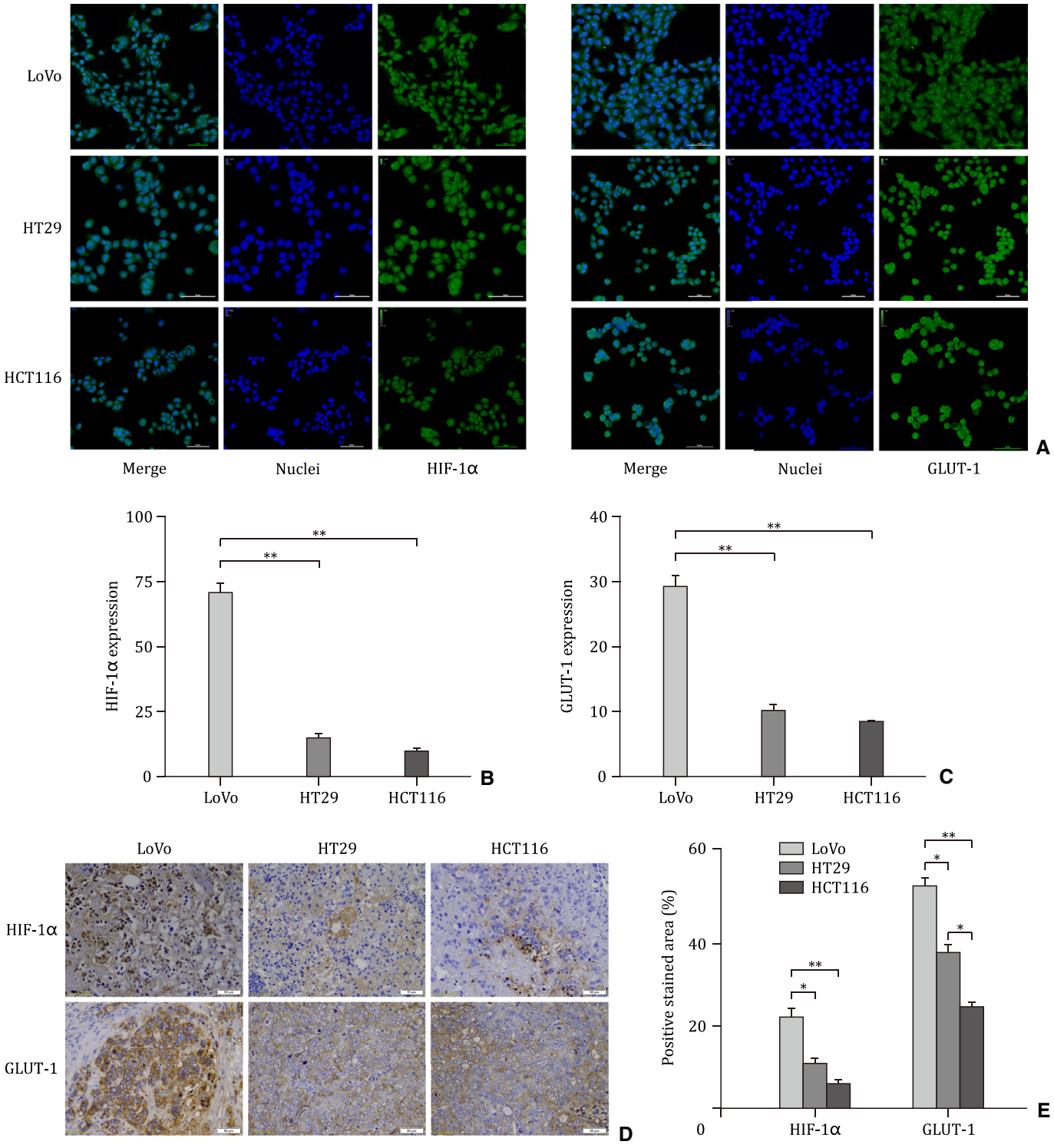

Fig. 4. Comparison of HIF-1α and GLUT-1 expression between LoVo, HT29 and HCT116 cells/tumor tissues. **A**: Micrographs of immunofluorescence staining for nuclei (blue) and HIF-1α/GLUT-1 (green) in LoVo, HT29 and HCT116 cells (original magnification $\times$ 200). **B** and **C**: Quantification of HIF-1α and GLUT-1 staining levels using Live Cell Imaging System. **D**: Immunohistochemical staining for GLUT-1/HIF-1α (brown) in LoVo, HT29 and HCT116 tumor-bearing tissues (original magnification $\times$ 200), respectively. **E:** Quantification of HIF-1α and GLUT-1 staining levels using Image-J software. Data are expressed as the mean $\pm$ standard deviation, * $P < 0.01$; ** $P < 0.001$.

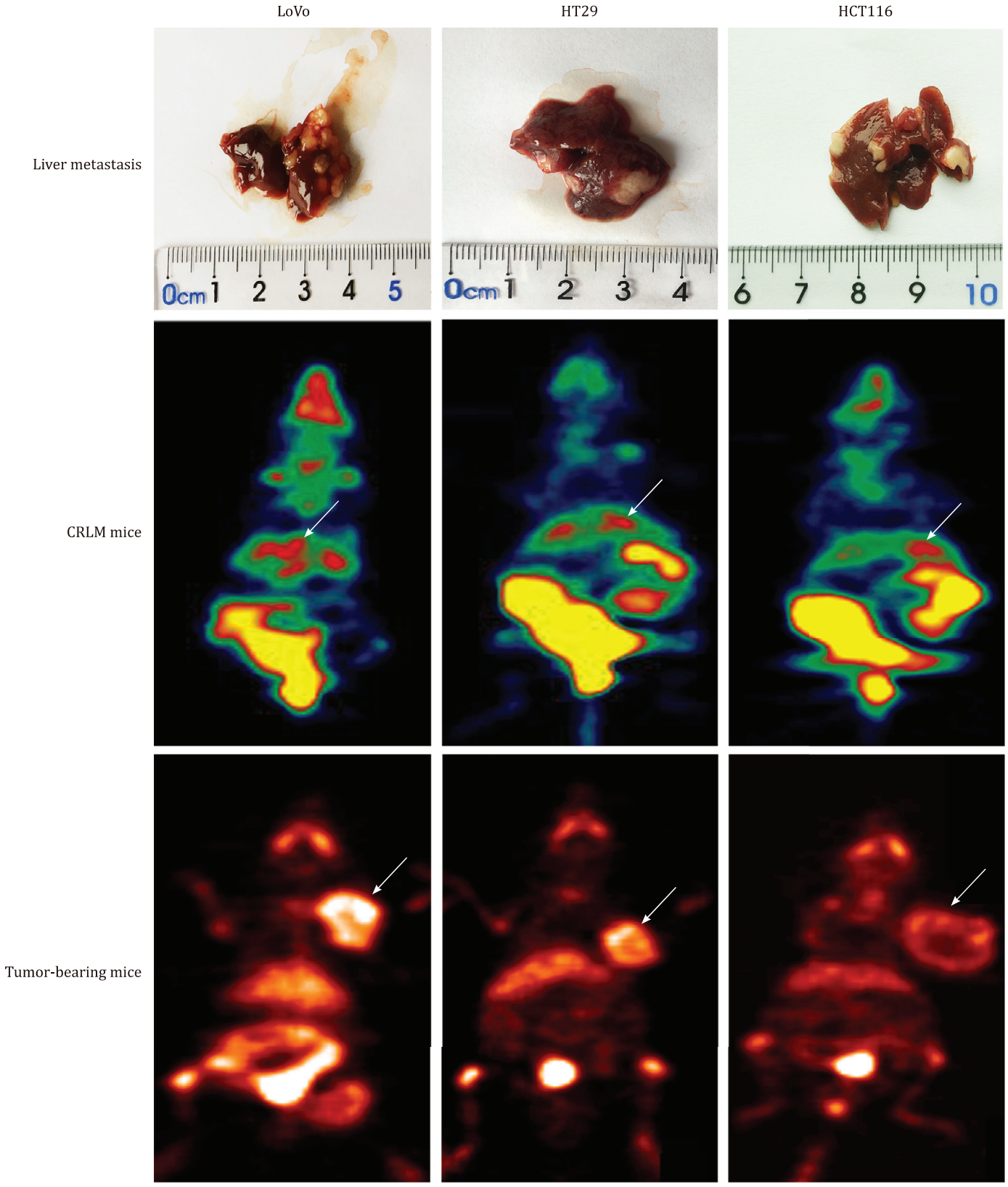

Fig. 5. Liver metastases anatomy pictures represent (from top to bottom), ^{18}F-FMISO liver metastases images and ^{18}F-FMISO tumor-bearing of LoVo, HT29 and HCT116 xenografts mice, respectively. Arrows indicate the uptake of ^{18}F-FMISO in tumor tissues.

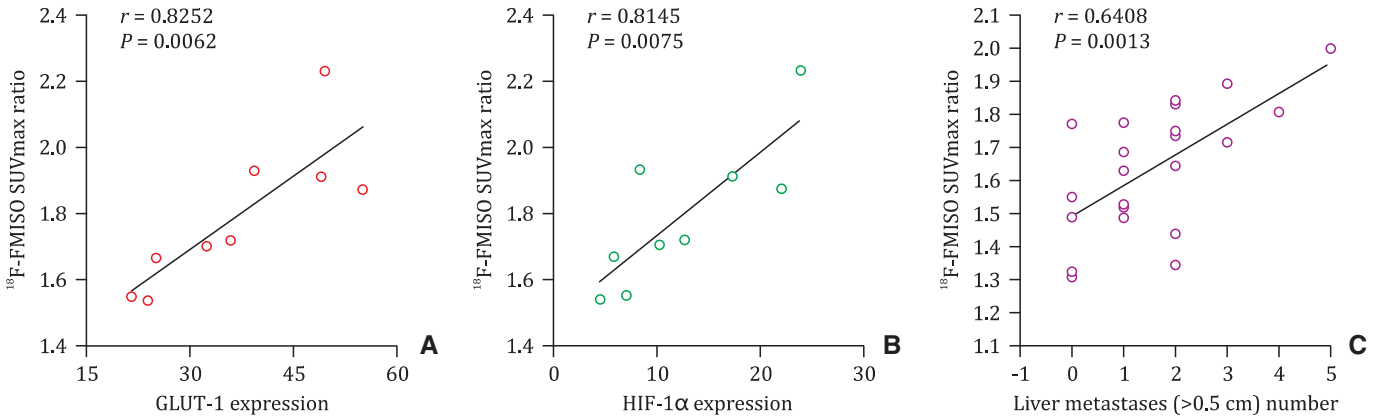

Fig. 6. Correlation analysis. **A** and **B**: A significant correlation was found between ^{18}F-FMISO SUVmax ratio and GLUT-1 and HIF-1α expression *in vivo*. **C**: A significant correlation was found between ^{18}F-FMISO SUVmax ratio and liver metastases number with the size larger than 0.5 cm.

distinguish protein expression heterogeneities in proteomics levels between tumors. However, only three CRC cell lines were not enough to represent the overall CRC. We plan to increase the variety of CRC cell lines in future experiments in order to comprehensively analyze the differences in biological characteristics in various CRC cell lines. In addition, CRC patients with or without liver metastases should be included in future trials to assess the clinical value of ^{18}F-FMISO PET quantitative parameter in predicting liver metastatic potential of CRC patients.

In conclusion, ^{18}F-FMISO parameter of SUVmax ratio may provide useful tumor biological information in mice with CRLM thus allowing for better prediction of CRLM and yielding useful radioactive markers for predicting liver metastatic potential in CRC.

Contributors

ZMY and JHJ proposed the study. ZMY and ZRJ performed the experiment and wrote the first draft. PWB, WYQ and LX collected and analyzed the data. JH and XHL participated in drafting and revising the manuscript. All authors approved the final version. JHJ is the guarantor.

Funding

This study was supported by grants from the National Natural Science Foundation of China (81471736, 81671760 and 81873910), Scientific Research Transformation Special Fund of Heilongjiang Academy of Medical Sciences (2018415), Scientific Research Project of Health and Family Planning Commission of Heilongjiang Province (CR201807).

Ethical approval

This study was approved by the Ethics Committee of the Second Affiliated Hospital of Harbin Medical University (KY2018-215). All micro-PET imaging procedures were conducted according to protocol approved by the Jiangsu Institute of Nuclear Medicine Animal Care and Use Committee.

Competing interest

No benefits in any form have been received or will be received from a commercial party related directly or indirectly to the subject of this article.

References

[1] Torre LA, Bray F, Siegel RL, Ferlay J, Lortet-Tieulent J, Jemal A. Global cancer statistics, 2012. CA Cancer J Clin 2015;65:87–108.
[2] Lam VW, Laurence JM, Pang T, Johnston E, Hollands MJ, Pleass HC, et al. A systematic review of a liver-first approach in patients with colorectal cancer and synchronous colorectal liver metastases. HPB Oxford 2014;16:101–108.
[3] Linnekamp JF, Wang X, Medema JP, Vermeulen L. Colorectal cancer heterogeneity and targeted therapy: a case for molecular disease subtypes. Cancer Res 2015;75:245–249.
[4] Sebagh M, Allard MA, Bosselut N, Dao M, Vibert E, Lewin M, et al. Evidence of intermetastatic heterogeneity for pathological response and genetic mutations within colorectal liver metastases following preoperative chemotherapy. Oncotarget 2016;7:21591–21600.
[5] Vaupel P, Harrison L. Tumor hypoxia: causative factors, compensatory mechanisms, and cellular response. Oncologist 2004;9:4–9.
[6] Ueda M, Saji H. Radiolabeled probes targeting hypoxia-inducible factor-1-active tumor microenvironments. Sci World J 2014;2014:165461.
[7] Pouysségur J, Dayan F, Mazure NM. Hypoxia signalling in cancer and approaches to enforce tumour regression. Nature 2006;441:437–443.
[8] Nagaraju GP, Bramhachari PV, Raghu G, El-Rayes BF. Hypoxia inducible factor-1α: its role in colorectal carcinogenesis and metastasis. Cancer Lett 2015;366:11–18.
[9] Asselin MC, O'Connor JP, Boellaard R, Thacker NA, Jackson A. Quantifying heterogeneity in human tumours using MRI and PET. Eur J Cancer 2012;48:447–455.
[10] Tesch G, Amur S, Schousboe JT, Siegel JN, Lesko LJ, Bai JP. Successes achieved and challenges ahead in translating biomarkers into clinical applications. AAPS J 2010;12:243–253.
[11] Rajendran JG, Krohn KA. F-18 fluoromisonidazole for imaging tumor hypoxia: imaging the microenvironment for personalized cancer therapy. Semin Nucl Med 2015;45:151–162.
[12] DeClerck K, Elble RC. The role of hypoxia and acidosis in promoting metastasis and resistance to chemotherapy. Front Biosci Landmark Ed 2010;15:213–225.
[13] Kelada OJ, Carlson DJ. Molecular imaging of tumor hypoxia with positron emission tomography. Radiat Res 2014;181:335–349.
[14] Fleming IN, Manavaki R, Blower PJ, West C, Williams KJ, Harris AL, et al. Imaging tumour hypoxia with positron emission tomography. Br J Cancer 2015;112:238–250.
[15] Spence AM, Muzi M, Swanson KR, O'Sullivan F, Rockhill JK, Rajendran JG, et al. Regional hypoxia in glioblastoma multiforme quantified with [18F]fluoromisonidazole positron emission tomography before radiotherapy: correlation with time to progression and survival. Clin Cancer Res 2008;14:2623–2630.
[16] Yamaguchi S, Hirata K, Toyonaga T, Kobayashi K, Ishi Y, Motegi H, et al. Change in 18F-fluoromisonidazole PET is an early predictor of the prognosis in the patients with recurrent high-grade Glioma receiving bevacizumab treatment. PLoS One 2016;11:e0167917.
[17] Cheng J, Lei L, Xu J, Sun Y, Zhang Y, Wang X, et al. 18F-fluoromisonidazole PET/CT: a potential tool for predicting primary endocrine therapy resistance in breast cancer. J Nucl Med 2013;54:333–340.
[18] Arvold ND, Heidari P, Kunawudhi A, Sequist LV, Mahmood U. Tumor hypoxia response after targeted therapy in EGFR-mutant non-small cell lung cancer: proof of concept for FMISO-PET. Technol Cancer Res Treat 2016;15:234–242.
[19] Norikane T, Yamamoto Y, Maeda Y, Kudomi N, Matsunaga T, Haba R, et al. Correlation of (18)F-fluoromisonidazole PET findings with HIF-1α and p53 expressions in head and neck cancer: comparison with (18)F-FDG PET. Nucl Med Commun 2014;35:30–35 .

[20] Bourdier T, Greguric I, Roselt P, Jackson T, Faragalla J, Katsifis A. Fully automated one-pot radiosynthesis of O-(2-[18F]fluoroethyl)-L-tyrosine on the TracerLab FX(FN) module. Nucl Med Biol 2011;38:645–651.
[21] Mojic M, Bogdanovic Pristov J, Maksimovic-Ivanic D, Jones DR, Stanic M, Mijatovic S, et al. Extracellular iron diminishes anticancer effects of vitamin C: an *in vitro* study. Sci Rep 2014;4:5955.
[22] Ding Z, Yang L, Xie X, Xie F, Pan F, Li J, et al. Expression and significance of hypoxia-inducible factor-1 alpha and MDR1/P-glycoprotein in human colon carcinoma tissue and cells. J Cancer Res Clin Oncol 2010;136:1697–1707.
[23] McMillan DC, McArdle CS. Epidemiology of colorectal liver metastases. Surg Oncol 2007;16:3–5.
[24] Manfredi S, Lepage C, Hatem C, Coatmeur O, Faivre J, Bouvier AM. Epidemiology and management of liver metastases from colorectal cancer. Ann Surg 2006;244:254–259.
[25] Kim TM, Jung SH, An CH, Lee SH, Baek IP, Kim MS, et al. Subclonal genomic architectures of primary and metastatic colorectal cancer based on intratumoral genetic heterogeneity. Clin Cancer Res 2015;21:4461–4472.
[26] Goranova TE, Ohue M, Shimoharu Y, Kato K. Dynamics of cancer cell subpopulations in primary and metastatic colorectal tumors. Clin Exp Metastasis 2011;28:427–435.
[27] Blanco-Calvo M, Concha á, Figueroa A, Garrido F, Valladares-Ayerbes M. Colorectal cancer classification and cell heterogeneity: a systems oncology approach. Int J Mol Sci 2015;16:13610–13632.
[28] Shweiki D, Itin A, Soffer D, Keshet E. Vascular endothelial growth factor induced by hypoxia may mediate hypoxia-initiated angiogenesis. Nature 1992;359:843–845.
[29] He F, Deng X, Wen B, Liu Y, Sun X, Xing L, et al. Noninvasive molecular imaging of hypoxia in human xenografts: comparing hypoxia-induced gene expression with endogenous and exogenous hypoxia markers. Cancer Res 2008;68:8597–8606.
[30] Zhao XY, Chen TT, Xia L, Guo M, Xu Y, Yue F, et al. Hypoxia inducible factor-1 mediates expression of galectin-1: the potential role in migration/invasion of colorectal cancer cells. Carcinogenesis 2010;31:1367–1375.
[31] Jung JH, Im S, Jung ES, Kang CS. Clinicopathological implications of the expression of hypoxia-related proteins in gastric cancer. Int J Med Sci 2013;10:1217–1223.
[32] Winnard PT Jr, Pathak AP, Dhara S, Cho SY, Raman V, Pomper MG. Molecular imaging of metastatic potential. J Nucl Med 2008;49 96S–112S.
[33] Estrella V, Chen T, Lloyd M, Wojtkowiak J, Cornnell HH, Ibrahim-Hashim A, et al. Acidity generated by the tumor microenvironment drives local invasion. Cancer Res 2013;73:1524–1535.
[34] Horsman MR, Mortensen LS, Petersen JB, Busk M, Overgaard J. Imaging hypoxia to improve radiotherapy outcome. Nat Rev Clin Oncol 2012;9:674–687.